ACS OMEGA

Open Access

http://pubs.acs.org/journal/acsodf

Article

Preparation of Coir Cellulose Nanofibers by Peroxyformic Acid Method and Their Application in Reinforced PVA Composite Films

Weishan Hou, Rui Teng, Aojia Zhang, Bang An, Mingcong Xu, Chunhui Ma, Gaofeng Pan,* Shouxin Liu,* and Wei Li*

Cite This: *ACS Omega* 2024, 9, 38205−38216

Read Online

ACCESS | Metrics & More | Article Recommendations

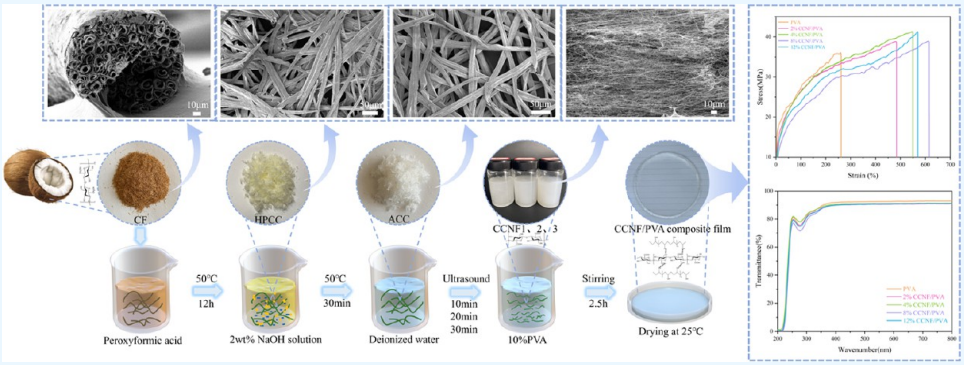

ABSTRACT: To increase the value of waste coconut shells and further broaden their use by biorefining, a milder and greener method to prepare cellulose nanofibers (CCNFs) was developed. The CCNFs were separated from coir fibers by using peroxyformic acid and alkali treatment in combination with high-power ultrasonication. The basic properties of the CCNFs were comprehensively evaluated using scanning and transmission electron microscopy, spectroscopy, diffraction, and thermogravimetric techniques. The results revealed that the developed preparation method provided CCNFs with typical nanocellulose sizes, structures, and properties. Nanocellulose-reinforced poly(vinyl acetate) (PVA) composite films were prepared using the CCNFs, and their mechanical properties, transmittance, crystallinity, and thermal stability were investigated. The elongation at break of the film with 8% CCNFs was 612%. The tensile strength of the films with 4 and 12% CCNFs was 41.3 MPa, which was higher than that of a PVA film (36 MPa). The transmittance and thermal stability of the PVA composite films were not appreciably affected by the CCNFs. The CCNFs show promise as a nanofiller for PVA-based composite films with favorable mechanical properties, crystallinity, and high transparency.

1. INTRODUCTION

Coconut is an important woody oil and fiber species in China.[1] Coconut plantations are mainly distributed in the tropical areas of South China and Southwest China, especially Hainan, where they are widely planted. Coir fiber (CF), as an accessory product of coconut, uses a considerable proportion of coconut shells each year. CF is mostly composed of cellulose (mass fraction of 46.0−63.0%), lignin (31.0−36.0%), hemicellulose (0.15−0.25%), and pectin (3.0−4.0%).[2] The high cellulose content and low hemicellulose content of CF endow it with excellent mechanical properties as well as high moisture and heat resistance.[3] CF also has the advantages of being renewable, abundant, and inexpensive, which make it an important raw material for the preparation of nanocellulose (NC).[4]

Although CF possesses a multitude of uses in numerous fields, its utilization rate is low. Thus, a large amount of CF is disposed of as waste each year, resulting in environmental pollution and a waste of biomass resources.[5] To address this, instead of using traditional wood-derived fiber for NC preparation, here, CF is used as the raw material to produce NC. Compared with wood-derived fiber, CF has a shorter growth cycle and higher abundance and may otherwise be a waste material. Thus, the use of CF instead of wood-derived fiber to produce NC will have positive effects on deforestation and climate change.

There are three main types of approaches to prepare NC: mechanical preparation methods,[4] e.g., high-pressure homog-

Received: June 20, 2024
Revised: August 16, 2024
Accepted: August 20, 2024
Published: August 28, 2024

Scheme 1. Overview of the Preparation Process of CCNFs and CCNF/PVA Composite Films

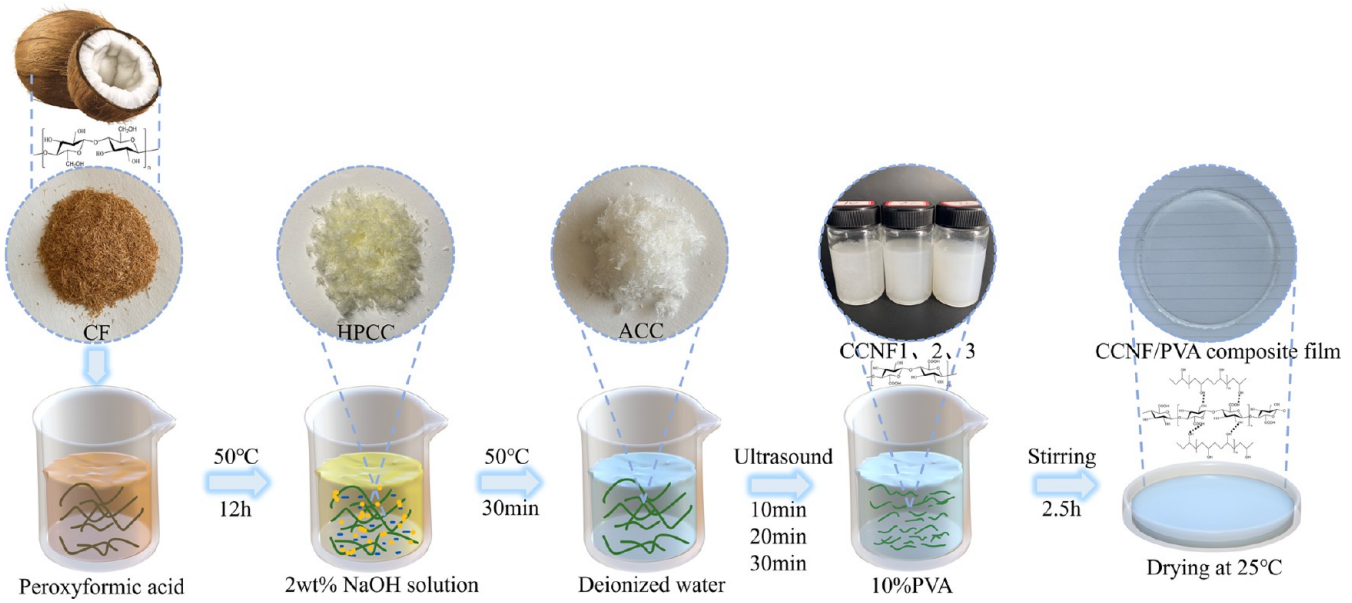

enization,[6] ball milling,[7] and ultrasonication;[8] chemical preparation methods, e.g., acid hydrolysis,[9] enzymatic hydrolysis,[10] and oxidation;[11] and solvent-based preparation methods, e.g., low-eutectic solvents[12] and ionic liquids.[13] The most commonly used technique to prepare cellulose nanofibers (CNFs) is oxidation using 2,2,6,6-tetramethylpiperidine-1-oxyl (TEMPO),[11,14] sodium chlorite,[15] or concentrated sulfuric acid.[16] Oxidation with these reagents provides rapid reaction, high crystallinity, and high yield, but there are still some problems associated with this approach. For example, the toxicity of TEMPO leads to environmental problems, the oxidation of the hydroxyl group of the primary alcohol on the C_6 position of cellulose is limited,[17] the equipment used for hydrolysis by an inorganic acid needs to be highly resistant to corrosion, the acid is not easy to recycle, and the reaction process generates chlorine gas that can pollute the environment.[18] In this investigation, coir cellulose nanofibers (CCNFs) were prepared from CF using peroxyformic acid, which produces hydroxyl and superoxide anion radicals, as well as a small content of sulfuric acid (H_2SO_4) to disrupt the aromatic ring and olefinic side chain of lignin, leading to its oxidative ring opening and cleavage.[19] The carboxyl groups produced during oxidation increase the solubility of lignin and hemicellulose in sodium hydroxide (NaOH) solution.[20] Most of the cellulose was isolated after the alkali treatment. Compared with previous studies,[11,18,21] this process is simpler and gentler.

Poly(vinyl alcohol) (PVA) is a biodegradable, nontoxic, and noncarcinogenic polymer[22] with good film-forming ability, favorable mechanical properties, and biocompatibility. However, the brittleness of PVA is high, so nanofillers such as graphene,[23] graphene oxide,[24] or carbon nanotubes[25] are often added to improve the stiffness of PVA nanocomposites. These nanofillers are difficult to degrade and make PVA less green. CNFs are frequently used as reinforcing materials to enhance the mechanical qualities of films because of their high crystallinity and renewability. Here, PVA films are prepared by adding CCNFs, providing composite films with decreased degradability and improved mechanical properties. The developed composite films are attractive as base materials for developing packaging materials with various functions.

The purpose of this study is to enhance the value of waste CF and further broaden its applications by developing a milder and greener method to prepare CCNFs (Scheme 1). The developed method selectively removes most of the lignin and hemicellulose from CF, enabling the isolation of CCNFs. The reinforcing properties of the CCNFs in PVA composite films are explored with the goal of developing advanced packaging materials.

2. MATERIALS AND METHODS

2.1. Materials. CF was purchased from the Taobao Dream Horticulture Brand Store. H_2O_2 (30%) was purchased from Tianjin Damao Chemical Reagent Factory. Formic acid (HCOOH, ≥88.0%) was purchased from Tianjin Fuyu Fine Chemical Co. Ltd. H_2SO_4 (95.0−98.0%) was acquired from Xilong Science Co. Ltd. NaOH was purchased from Tianli Chemical Reagent Co. Ltd. PVA with a degree of polymerization of 1788, alcoholysis of 87.0−89.0 mol %, and viscosity of 3.2−3.6 mPa·s was obtained from Macklin. Deionized water was used in all of the experiments.

2.2. Preparation of Peroxyformic Acid. 200 mL of the 30% hydrogen peroxide solution was slowly added to HCOOH (200 mL) with stirring, and then concentrated H_2SO_4 (2.6 g, 1% of the total mass of H_2O_2 and HCOOH) was added. The reaction mixture was stirred for 1 h to form a 10 v/v % solution of peroxyformic acid.

2.3. Delignification. CF (4 g) was immersed in a peroxyformic acid solution (400 mL) and reacted in a water bath at 50 °C for 12 h to selectively decompose lignin and hemicellulose, giving coir cellulose heated with peroxyformic acid (HPCC). HPCC was neutralized by addition to 2 wt % NaOH solution (200 mL) in a water bath at 50 °C for 30 min to remove any remaining lignin and hemicellulose. The material was repeatedly cleaned with deionized water until the pH was neutral to remove any traces of chemicals from the treated CF, giving alkali-treated coir cellulose (ACC).

https://doi.org/10.1021/acsomega.4c05759
ACS Omega 2024, 9, 38205−38216

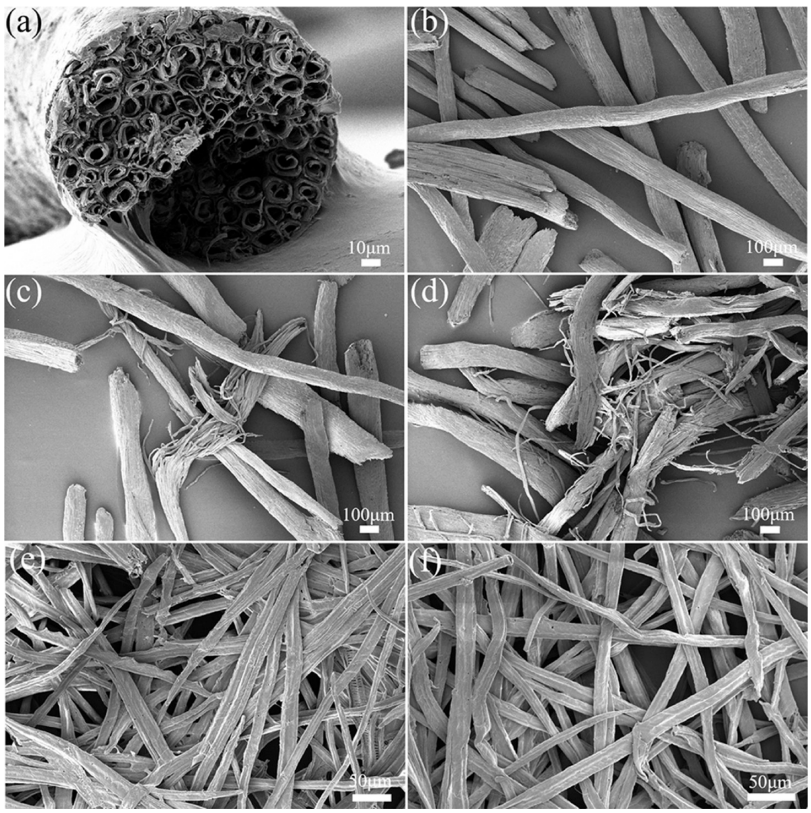

Figure 1. SEM images of (a) the cross section of a CF, (b) untreated CF, CF after peroxyformic acid treatment for (c) 4 and (d) 8 h, (e) HPCC, and (f) ACC.

2.4. Preparation of Cellulose Nanofibers. ACC (1.2 g) was dispersed in deionized water (200 mL) and subjected to intermittent high-intensity ultrasound at 1000 W for 10, 20, or 30 min. Each ultrasonication cycle lasted 0.2 s and included 0.1 s of ultrasonication and 0.1 s without ultrasonication. Ultrasonication for 10, 20, and 30 min provided the CCNF samples denoted as CCNF-1, CCNF-2, and CCNF-3, respectively.

2.5. Preparation of PVA Composite Films. PVA composite films were made by a solution casting technique. PVA solution (10% w/v) was combined with a certain amount of CCNF-3 suspension (0, 2, 4, 8, or 12% w/w with respect to PVA), and then, the mixture was stirred for 2.5 h. After removal of air bubbles, the slurry was poured into a sanitized casting mold and then dried at 25 °C for 36 h to produce a composite film. The composite films produced using 0, 2, 4, 8, and 12% (w/w) CCNF-3 are denoted as PVA, 2% CCNF/PVA, 4% CCNF/PVA, 8% CCNF/PVA, and 12% CCNF/PVA, respectively.

2.6. Characterization. The CCNF yield was calculated based on the ratio of the final mass of the fibers after preparation to the initial mass of CF.[26] The Klason lignin, hemicellulose, and α-cellulose contents were determined based on the criteria outlined in the TAPPI T19 m-54 standard and by Li,[27] respectively.

The surface morphology and cross section of samples were observed by scanning electron microscopy (SEM; Thermo Scientific). Transmission electron microscopy (TEM; JEM-2100, JEOL, Japan) was employed to characterize the morphology of each fiber sample. The test samples were stained with uranyl acetate, and then dispersions were added dropwise onto a copper mesh. The dispersions of CCNFs were observed at an accelerating voltage of 120 kV. The morphology and size of cellulose nanofibers were observed by using atomic force microscopy (AFM) (Bruker Dimension Icon, Germany).

The ζ-potential of CCNF aqueous suspensions was measured using a Zeta sizer Nano ZSE (Malvern Instruments Ltd., Worcestershire, U.K.) after 10-fold dilution with distilled water. The carboxyl group content in the fibers was determined by a titrimetric analysis. CCNF was dissolved at reflux in a mixed solvent of phenol-trichloromethane and titrated with a standard titrimetric solution of potassium hydroxide-ethanol, and a blank test was done under the same conditions. The content of terminal carboxyl groups was calculated from the number of volumes of the standard titration solution consumed.

Fourier transform infrared (FT-IR) spectroscopy (Thermo Nicolet, Massachusetts) was used to analyze the functional groups in the samples after each reaction step. FT-IR spectra were measured in the wavenumber range from 500 to 4000 cm^{-1}. Powder X-ray diffraction (XRD) measurements were conducted on a 20161262 X'Pert3 diffractometer at a tube current of 40 mA and tube pressure of 40 kV. Measurements were conducted between 10 and 40° at a scan rate of 4°/min. For each sample examined, the crystallinity index [CrI (%)] was determined using the technique outlined by Segal et al.,[28]

$$\mathrm{CrI}(\%) = [(I_{200} - I_{\mathrm{am}})/I_{200}] \times 100 \quad (1)$$

The thermal stability of samples in a nitrogen atmosphere was determined by thermogravimetric analysis (TGA; TA Discovery TGA 550) and differential thermogravimetry (DTG). Samples were heated at a rate of 10 °C/min in the temperature range from 30 to 700 °C. The transmittance of the composite films was measured by ultraviolet−visible (UV−vis) spectros-

https://doi.org/10.1021/acsomega.4c05759
ACS Omega 2024, 9, 38205−38216

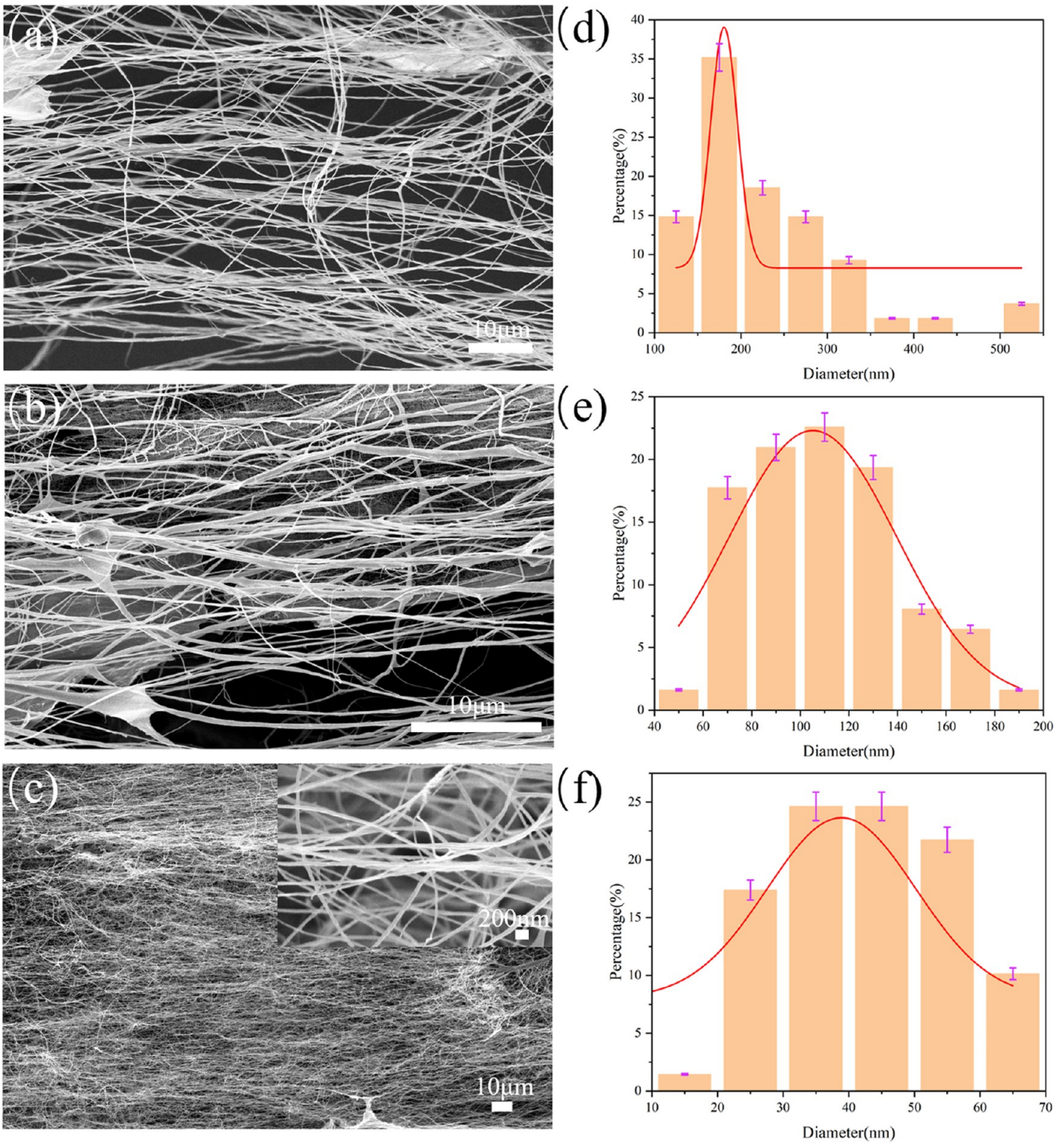

Figure 2. SEM images of (a) CCNF-1, (b) CCNF-2, and (c) CCNF-3. Size distributions of the fiber diameters of (d) CCNF-1, (e) CCNF-2, and (f) CCNF-3.

copy (Hitachi U4150, Japan) in the wavelength range of 200−800 nm. The mass, dimensions, and thickness of the composite films were quantified using an analytical balance and digital vernier calipers to calculate the film density and moisture content. Three distinct points were measured in parallel for each film. The differential scanning calorimetry (DSC) curves of the composite films were measured using a differential scanning calorimeter (TA Q20), ramping up from 30 to 230 °C, cooling down to 20° holding for 5 min, and then repeating. The crystallinity of the composite films was calculated according to the published formula.[29] The tensile strength and elongation at break of the composite films were measured by an electronic universal testing machine (Instron 5982/8872/CMT4104/RGM-6300). Each measurement was repeated three times at a loading rate of 20 mm/min.

3. RESULTS AND DISCUSSION

3.1. Morphological and Component Analyses. An SEM image of the cross section of a CF, which is made up of tubular fibers and an intercellular matrix, is depicted in Figure

https://doi.org/10.1021/acsomega.4c05759
ACS Omega 2024, 9, 38205−38216

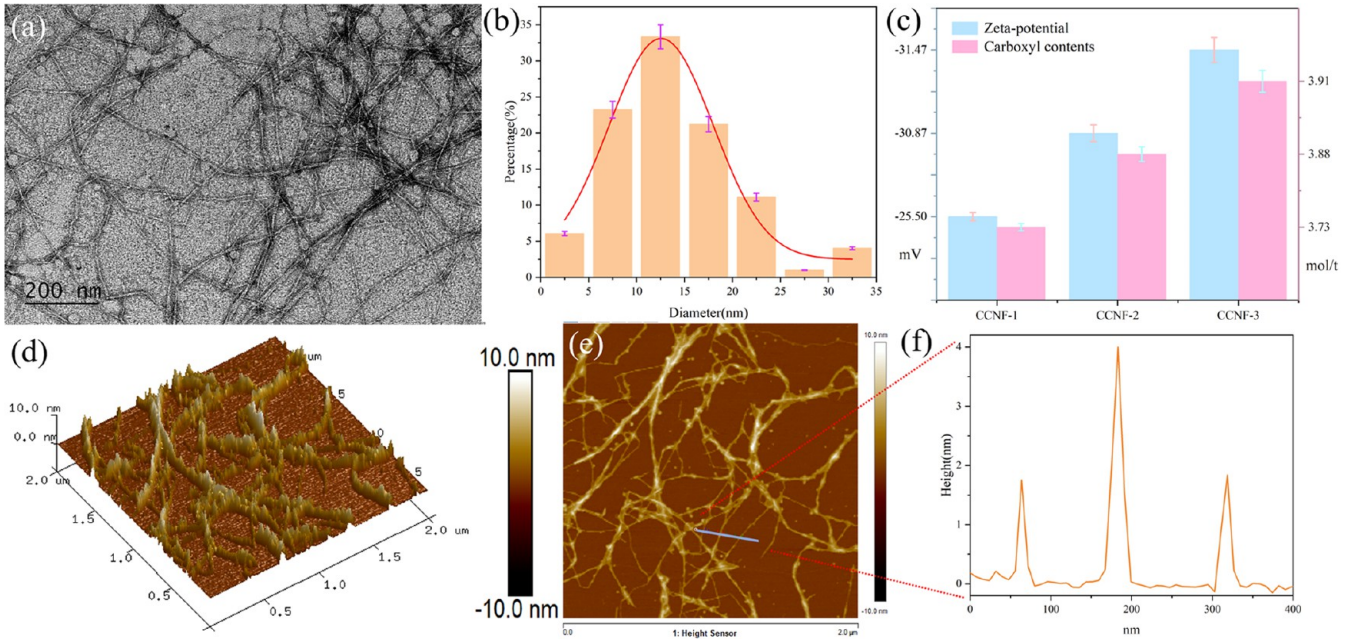

Figure 3. (a) TEM image of CCNF-3. (b) Diameter-size distribution of CCNF-3. (c) ζ-Potential and carboxyl contents of CCNF. (d–e) AFM image of CCNF-3, and (f) cross-sectional contours of CCNF-3.

1a. The tubular fibers with different morphologies and sizes are arranged in parallel, forming a hollow structure. Figure 1b shows that the surface of the raw CF is rough because it is covered by noncellulosic materials and has many pits and impurities. After the delignification of the CF with peroxyformic acid for 4 h, individual fibers were partially separated (Figure 1c). The reaction area gradually enlarged, and a disorganized structure appeared after reaction for 8 h (Figure 1d). After 12 h of reaction, most of the fibers had separated, and the structure was completely disordered (Figure 1e). This behavior was ascribed to lignin and hemicellulose being partially destroyed by peroxyformic acid, which caused the fiber structure to degrade and become less ordered. However, because hemicellulose and lignin were not entirely removed, many fiber bundles remained intact. Alkali treatment further weakened the interactions among hemicellulose, lignin, and cellulose, resulting in complete dispersion of separated fibers (Figure 1f).

Figure 2a–c shows the fibers after high-power ultrasonic treatment, which broke up the individual fibers into nanoscale products. With a lengthening of the ultrasonic treatment duration, the dispersion of nanofibers increased. According to Figure 2d, the diameter of individual fibers in CCNF-1 ranged from 100 to 500 nm with an average diameter of 180.5 ± 354.28 nm. The diameter of individual fibers in CCNF-2 ranged from 40 to 200 nm with an average diameter of 105.2 ± 4.98 nm (Figure 2e). The diameter of individual fibers in CCNF-3 was 5–70 nm with an average diameter of 38.9 ± 6.16 nm (Figure 2f). These values indicate that the nanofibers gradually fragmented and dispersed into finer fibers as the ultrasonic treatment duration increased. In addition, CCNF-1 and CCNF-2 had diameter distributions wider than that of CCNF-3, which is likely caused by the incomplete fragmentation effect of ultrasound on the fibers at a shorter treatment duration.

Figure 3a shows the TEM image of CCNF-3, Figure 3d shows the AFM height image of CCNF-3, and Figure 3e shows its AFM planar image. It can be clearly observed by SEM, TEM, and AFM images that the fibers are well individualized to nanosize. And there is no particularly obvious bonding or aggregation, and the cellulose nanofibers are uniform in size and well separated. This is because the anionically charged CCNFs repel one another electrostatically, as evidenced by their high negative ζ-potential of approximately −31.47 ± 0.9 mV (Figure 3c).[3] Figure 3c shows the ζ-potential and carboxyl contents of CCNF. The carboxyl content of CCNF-1 was 3.98 ± 0.15 mol/t, indicating that the oxidative behavior of the fibers occurred during the delignification process. The XRD results indicate that the crystal shape of the fibers retained the cellulose I crystal structure after the treatment, suggesting that no oxidation occurred within the crystals. The carboxyl group of CCNF is likely derived from the selective oxidation of the C6 primary hydroxyl group on the surface of cellulose microfibers or cellulose microcrystals by peroxyformic acid.[30] Therefore, the negative ζ-potential of CCNF-1 is predominantly attributed to the dissociated carboxyl groups. However, with the prolongation of sonication time, the negative potential of CCNF gradually increased, and the carboxyl group contents of CCNF became relatively small. This indicates that with deeper ultrasonic depth, the fiber filaments are more finely divided and more free carboxyl group and hydroxyl group are exposed. Consequently, the negative potential rises and the fiber becomes more stable.

Due to the relatively low resolution of SEM, there is a tip-broadening effect in the measurements.[26] The diameter of CCNF-3 analyzed by TEM images is similar to that of SEM or even finer, being able to reach 12.5 ± 1.7 nm. According to the AFM images, the curves shown in Figure 3f correspond to the cross-sectional contours marked with blue lines in Figure 3e. The bottom of the morphology contour and the horizontal and vertical coordinates of Figure 3f correspond to the cross-sectional length and height of the defined structure, respectively. The diameter of CCNF-3 is derived from the cross-sectional length, which is roughly 34.66 ± 12.22 nm.

https://doi.org/10.1021/acsomega.4c05759
ACS Omega 2024, 9, 38205−38216

Table 1. Chemical Composition and Yield of CF, HPCC, ACC, CCNF-1, CCNF-2, and CCNF-3

samples	α-cellulose (%)	hemicelluloses (%)	Klason lignin (%)	acid-soluble lignin (%)	yields (%)
CF	31.47 ± 0.25	30.40 ± 0.26	33.47 ± 0.06	2.00 ± 0.10	
HPCC	43.80 ± 0.3	40.77 ± 0.25	12.33 ± 0.25		67.88 ± 0.01
ACC	72.33 ± 0.4	19.53 ± 0.15	2.47 ± 0.3		60.78 ± 0.06
CCNF-1	70.63 ± 0.4	19.33 ± 0.25	2.37 ± 0.5		53.01 ± 0.04
CCNF-2	71.07 ± 0.6	19.23 ± 0.21	2.37 ± 0.21		53.02 ± 0.7
CCNF-3	71.07 ± 0.3	19.20 ± 0.3	2.43 ± 0.06		52.95 ± 0.33

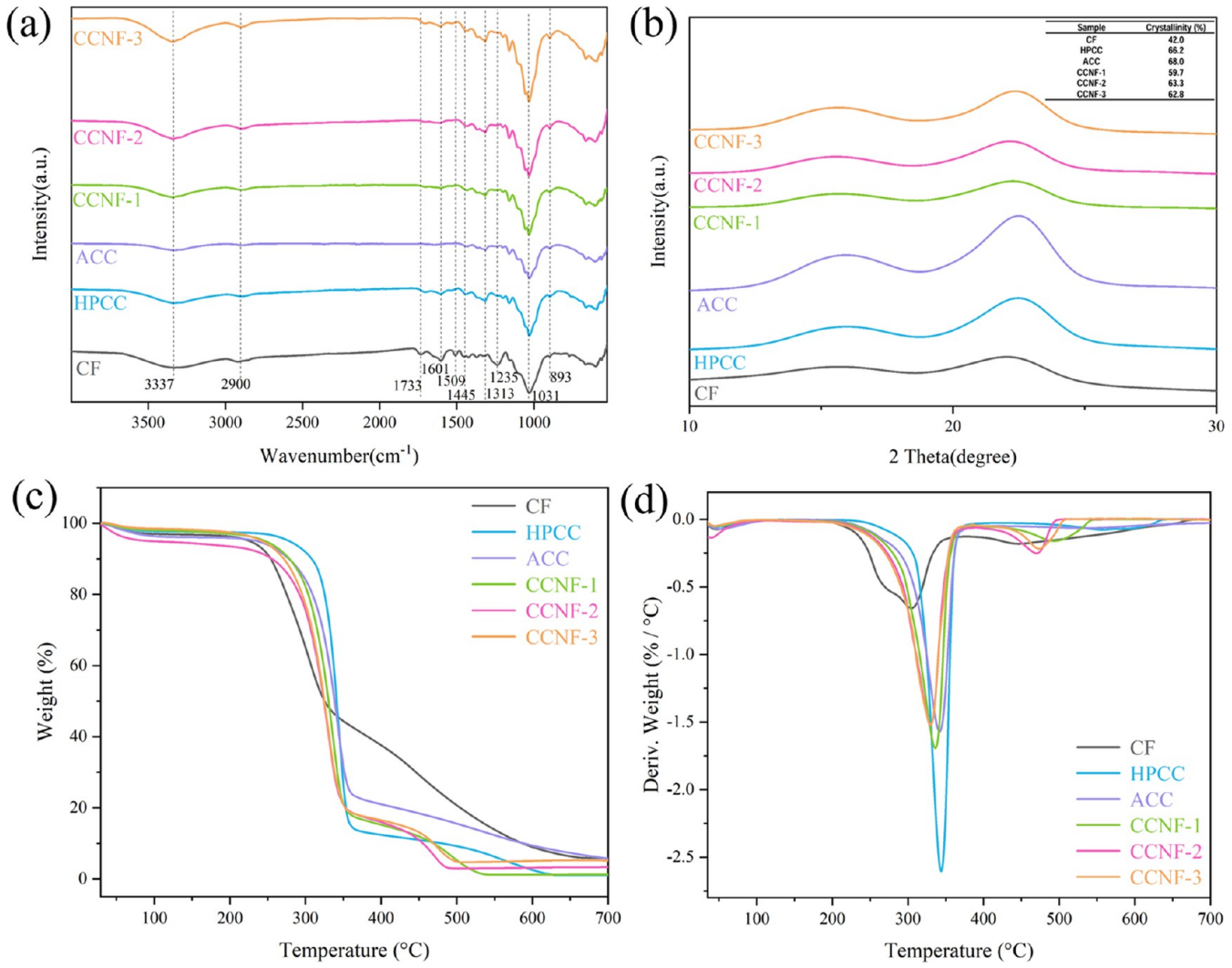

Figure 4. (a) FT-IR spectra, (b) XRD patterns and crystallinity, (c) TGA profiles, and (d) DTG profiles of fiber samples.

This is in accordance with the results of both SEM and TEM analyses. Diameter analyses by SEM, TEM, and AFM are all important owing to the limitations of analytical sampling and measurement errors of the instruments.

The exact length of CCNF cannot be precisely measured due to fiber aggregation and overlap caused by interfiber hydrogen bonding. According to Figure 3d, it can be predicted that CCNF-3 has a length of a few micrometers, and thus the length-to-diameter ratio of the isolated CCNF is expected to be very high. The length-to-diameter ratio of CNFs directly affects their mechanical stress distribution in composites; the larger the CNF length-to-diameter ratio, the better the strength and mechanical properties of composites.[31] Therefore, CCNF-3 is more likely than CCNF-1 and CCNF-2 to meet the requirements for use as a reinforcement material.

3.2. Structural and Component Analyses. The yields of HPCC, ACC, and CCNFs based on the dry weight of CF are listed in Table 1. The yield of CCNFs was approximately 53.01 ± 0.04%, which is higher than that achieved in previous studies on coir NC formation.[21,32] The changes in the chemical constitution of the fiber samples throughout the treatment process are summarized in Table 1. CF contained considerable proportions of α-cellulose (31.47%) and lignin (33.47% of Klason lignin and 2% of acid-soluble lignin), accompanied by a relatively low content of hemicellulose (30.4%), consistent with a previous report.[15] The Klason lignin content of HPCC was 12.33%; this decrease from that of CF was attributed to

https://doi.org/10.1021/acsomega.4c05759
ACS Omega 2024, 9, 38205−38216

the decomposition of lignin by peroxyformic acid. Conversely, the hemicellulose content of HPCC increased (40.77%) compared with that of CF, which was ascribed to peroxyformic acid only partially decomposing hemicellulose so that it remained attached to the fibers. Following alkali treatment to form ACC, the hemicellulose and Klason lignin contents decreased to 19.53 and 2.47%, respectively, whereas the α-cellulose content increased to 72.33%. These results suggest that the alkali treatment effectively purified the fibers. Following ultrasonic treatment, the components underwent minimal alteration, suggesting that ultrasound had a negligible effect on the chemical composition of the cellulose fibers. The relatively minor discrepancy in content between CCNF-1, CCNF-2, and CCNF-3 was attributed to the influence of ultrasound on the physical morphology of the fibers and crystalline regions.

FT-IR spectra of the fiber samples are shown in Figure 4a. The strong peak around 3337 cm^{-1} was assigned to the O−H stretching vibration, the peak near 2900 cm^{-1} was ascribed to the C−H stretching vibration, the peak at 1031 cm^{-1} was assigned to the C−O bond of cellulose,[33] and the peak at 893 cm^{-1} was consistent with the deformation vibration of cellulose C−H. The FT-IR spectra of the six samples (Figure 4a) all contained these characteristic peaks, which indicates that although the delignification and ultrasonic treatment of CF caused morphological changes, the functional components on the outermost layer of the fibers remained unchanged. Compared with CF, the stretching vibration of cellulose CH_2 around 1313 cm^{-1} and the bending vibration of cellulose C−H around 1445 cm^{-1} became more obvious after delignification (i.e., for HPCC). The peak around 1733 cm^{-1} originating from the ester bond of carboxylic acid groups of lignin or hemicellulose decreased in intensity after delignification, indicating that lignin and hemicellulose were partially removed.[9,34] In addition, the presence of characteristic peaks of hemicellulose at 1733 and 1240 cm^{-1} and the aromatic C=C ring vibrations of lignin at around 1601 and 1509 cm^{-1} indicated that HPCC still contained lignin and hemicellulose.[35,36] The absence of peaks at 1733, 1601, 1509, and 1240 cm^{-1} in the FT-IR spectra of ACC and the CCNFs indicated that the alkali treatment mostly removed lignin and hemicellulose.

Figure 4b shows the XRD patterns of CF, HPCC, ACC, CCNF-1, CCNF-2, and CCNF-3. The XRD pattern of CF contained a diffraction peak near $2\theta = 22°$, indicating that CF had the cellulose I crystal structure along with some impurity peaks. After delignification, alkali treatment, and ultrasonication, diffraction peaks were observed near 2θ = 16.5 and 22°. These two distinct diffraction peaks indicate that the CCNFs also had a cellulose I crystal structure.

The crystallinity of the samples (inset of Figure 4b) was calculated using a reported technique.[28] The crystallinity of CF was 42% and increased to 66.2% after delignification, indicating that a large amount of lignin was removed in the formation of HPCC. After alkali treatment, the crystallinity of ACC was 68%, indicating that some of the amorphous hemicellulose was removed by this process. The intensities of crystalline and amorphous peaks of samples decreased following ultrasonication, and the crystallinity of CCNF-1 was 59.7%. This is because ultrasound is nonselective and damages both amorphous and crystalline regions.[37] The crystallinity of CCNF-2 subjected to ultrasonication for 10 min increased to 63.3%, which is because the crystalline regions were damaged more slowly than the amorphous areas.[38] When the ultrasonic treatment time was extended to 30 min, the crystallinity of CCNF-3 decreased slightly to 62.8%, indicating that the crystalline areas began to degrade. Therefore, ultrasonication at an output power of 1000 W for 20 min provided CCNFs with a relatively high crystallinity. The crystallinity of the CCNFs was higher than that of coir NC prepared by TEMPO-mediated oxidation.[11]

3.3. Thermal Stability. The thermal stability of the fiber samples was analyzed by both TGA (Figure 4c) and DTG (Figure 4d). The weight loss below 100 °C was ascribed to adsorbed water evaporating from the samples. According to Table 2, showing onset temperature and T_{max} (degradation temperature) of the samples, CF exhibited two main degradation phases, and the three peaks in its DTG curve (T_{max} = 49, 304, and 454 °C) corresponded to these phases. The first stage was mainly attributed to the thermal depolymerization of hemicellulose, which has lower thermal stability than lignin and cellulose.[39,40] The second stage from 330 to 450 °C involved the degradation of lignin and cellulose, which showed lower heat loss than hemicellulose degradation and covered a relatively wide temperature range. These features were consistent with the higher thermal stability of lignin compared with that of carbohydrates.[41]

Table 2. Onset Temperature and Degradation Temperature (T_{max}) of CF, HPCC, ACC, CCNF-1, CCNF-2, and CCNF-3

	first process	second process		third process	
samples	T_{max} (°C)	onset temperature (°C)	T_{max} (°C)	onset temperature (°C)	T_{max} (°C)
CF	49.17	257.47	304.01	423.16	453.61
HPCC	46.82	324.20	343.76	515.64	557.36
ACC	55.36	310.46	341.81	482.42	544.23
CCNF-1	45.55	304.74	335.92	461.81	494.70
CCNF-2	42.61	297.51	329.76	444.02	470.54
CCNF-3	43.04	295.25	330.08	451.02	473.71

HPCC and ACC also had a three-stage degradation process. The peak at 343 °C in the corresponding DTG curves was also consistent with this stage. The heat loss was lower than that of CF, which indicated that HPCC and ACC showed high thermal stability. These results suggest that delignification and alkali treatment effectively removed a large amount of lignin and hemicellulose from CF.

The TGA and DTG curves of CCNF-1, CCNF-2, and CCNF-3 contained two characteristic decomposition stages, which was consistent with the earlier findings indicating that high-power ultrasound had minimal effect on the thermal stability of CCNFs.[42] Considering the results of FT-IR spectroscopy, XRD, and morphological characterization, the length of ultrasonic treatment time does not affect the chemical composition and thermal stability of the CCNFs, but only their structure.

As the sonication period increased, the temperature range of the second stage narrowed. This was attributed to the intermolecular hydrogen bonding in the CCNFs being disrupted to a certain extent by delignification and sonication. The smaller the size of the resulting fibers, the larger the exposed surface area, making the CCNFs with smaller transverse dimensions more susceptible to degradation at high temperatures than those with larger diameters.[11,36]

https://doi.org/10.1021/acsomega.4c05759
ACS Omega 2024, 9, 38205−38216

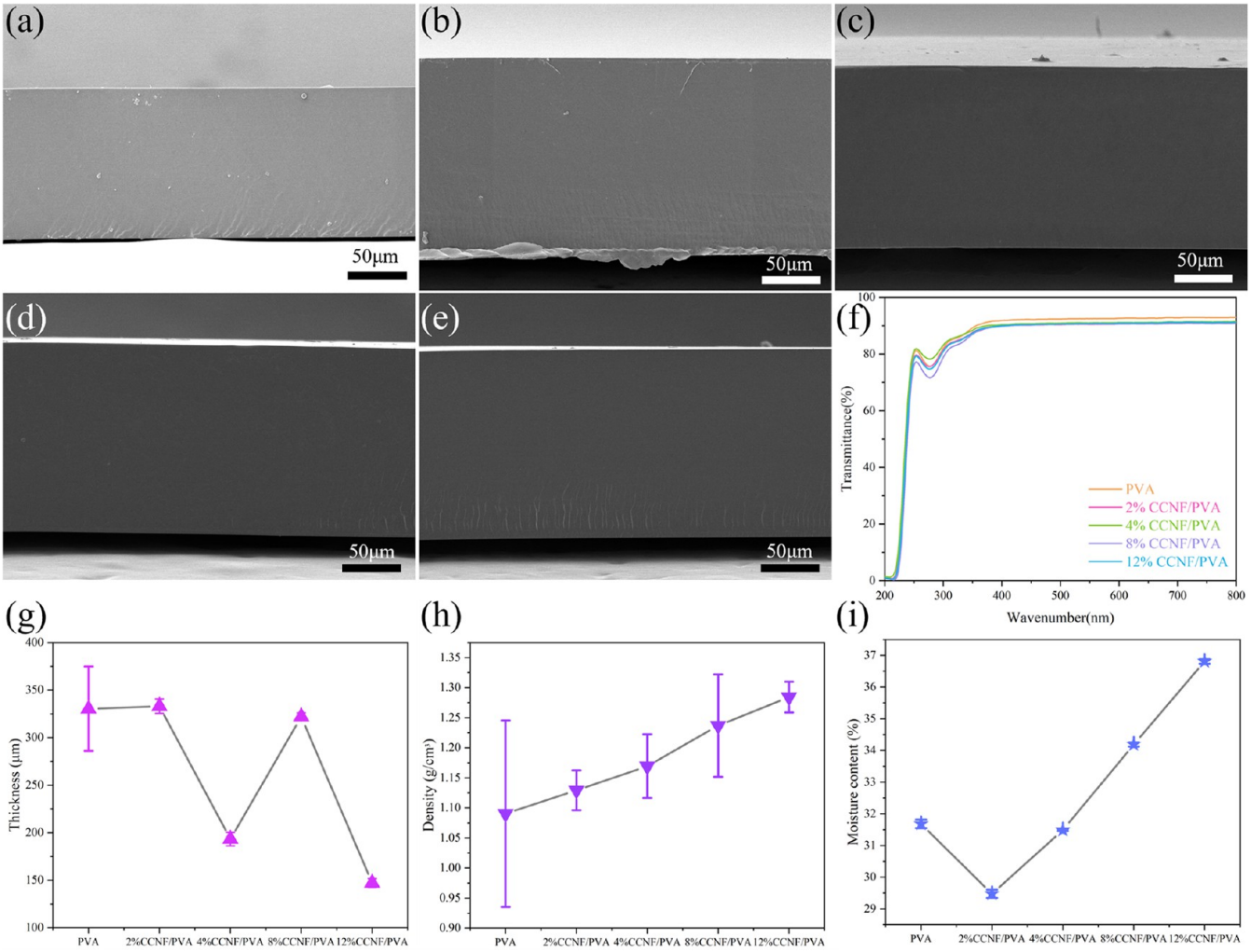

Figure 5. Cross-sectional SEM images of (a) PVA, (b) 2% CCNF/PVA, (c) 4% CCNF/PVA, (d) 8% CCNF/PVA, and (e) 12% CCNF/PVA films. (f) Transmittance spectra, (g) thickness, (h) density, and (i) moisture content of composite films.

Moreover, the thermal stability of coir nanocellulose prepared by the method of peroxyformic acid combined with high-power ultrasound was superior compared to previous nanocellulose methods.[11,21]

3.4. Morphology of Composite Films. Figure 5a−e shows SEM images of the cross sections of the composite films. As the CCNF content increased, the exposed surfaces of all of the films remained uniform, indicating that CCNFs and PVA showed good compatibility and that CCNFs can be uniformly dispersed in PVA-based films.

The transmittance of the films in the wavelength range of 200−800 nm is shown in Figure 5f. The addition of CCNFs to PVA led to a decrease in the transmittance of the films from 92.95% (PVA) to 91.08% (12% CCNF/PVA), which is a decrease of only 1.87%. The transmittance of the films with 2, 4, 8, and 12% CCNFs was fairly similar to that of an undoped PVA film, which shows that the CCNFs had a small effect on the ability of the PVA-based films to transmit visible light. The limited effect of the CCNFs on the visible-light transmission of the composite films indicates that the CCNFs were well dispersed in PVA and the composite films are attractive for use as packaging materials with high transparency.

3.5. Physical Properties of Composite Films. The physical properties of the films are presented in Figure 5g,h. The films became thinner with an increasing CCNF content. This phenomenon can be attributed to the CCNFs promoting the formation of dense nanonetworks in the composite films.[43] The density of the films gradually increased with the CCNF content, indicating that CCNFs were uniformly dispersed within the PVA matrix. However, at a CCNF content of 12%, the film thickness began to increase and its density decreased slightly. This is likely related to the high concentration of CCNFs resulting in an increase in their aggregation in the film and a more uneven distribution compared with that in CCNF/PVA films with a lower CCNF content.

The moisture content of the films is summarized in Figure 5i. Overall, there is minimal variation in water content between the composite films, which is because the CCNFs do not markedly alter the internal microstructure of PVA. The variation in water content may be attributed to the formation of hydrogen bonds between PVA and CCNF, which results in a decrease of the number of free hydroxyl groups in PVA, consequently leading to a decrease in its affinity for water molecules.[32,44]

3.6. Crystalline Structure of Composite Films. Figure 6a depicts the XRD patterns of the composite films. All films exhibited a distinctive peak at 19.4° that corresponded to the (101) plane of semicrystalline PVA.[43−45] The diffractogram of

https://doi.org/10.1021/acsomega.4c05759
ACS Omega 2024, 9, 38205−38216

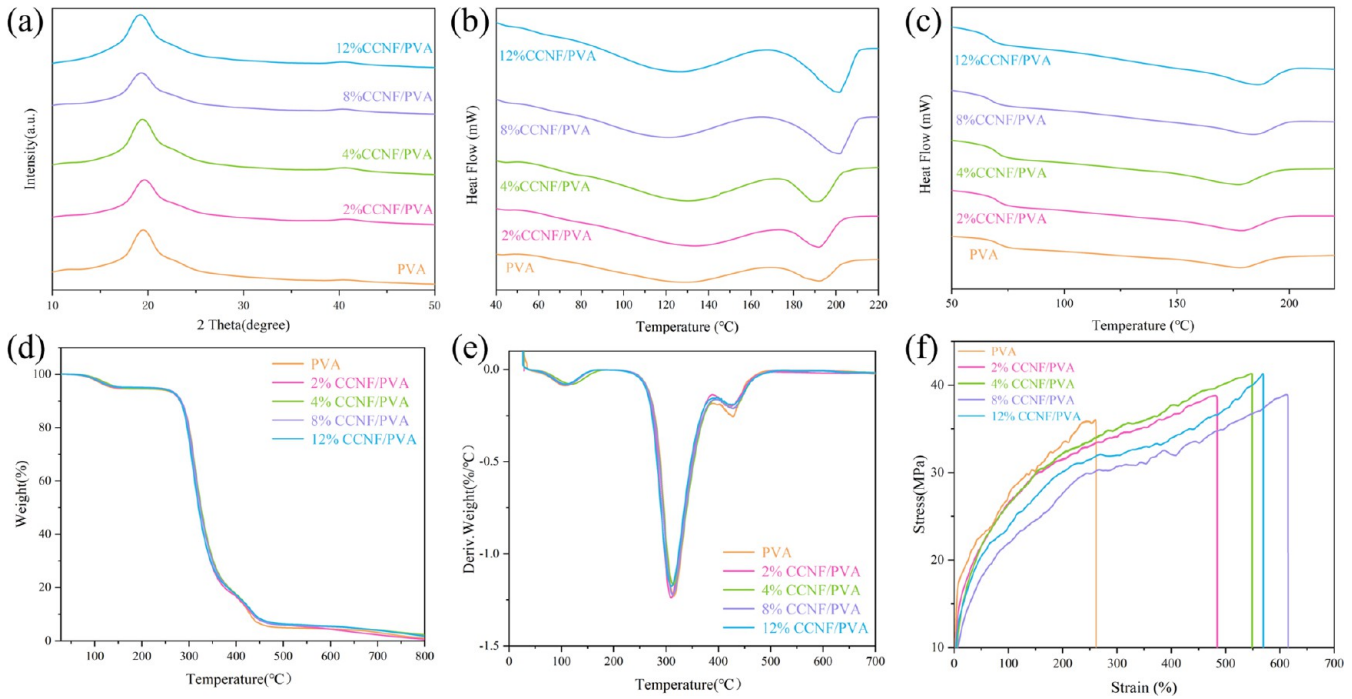

Figure 6. (a) XRD patterns, and DSC profiles of different composite films in (b) first heating and (c) second heating. (d) TGA profiles, (e) DTG profiles, and (f) mechanical properties of composite films.

the 8% CCNF/PVA film also exhibited this peak, albeit widened, indicating an increase in the crystallinity of the composite film. This observation is corroborated by the TGA/DTG results. A weaker diffraction peak was observed at 40.5°, which is also characteristic of PVA. This suggests that the physical or chemical interaction between CCNF and PVA does not disrupt the basic crystalline structure of PVA. PVA exhibits a smaller crystalline peak at 11.5°;[43,45] the intensity of this peak diminishes as the CCNF content increases. In the absence of intermolecular interactions between polymeric components, the crystalline regions of each component are particularly prominent in a composite.[45] It can thus be concluded that the lower intensity of the diffraction peak at 11.5° and the weak cellulose characteristic peaks in the composite films are primarily caused by the sufficiently homogeneous dispersion of CCNFs in the PVA matrix and the interaction between CCNF and PVA.

Figure 6b illustrates the differential scanning calorimetry (DSC) curves of the composite films during the initial heating cycle. A specific heat increment was observed at approximately 70 °C, which corresponds to the glass transition temperature (T_g) of PVA.[29] The lower the T_g of the composite film as the amount of CCNF addition increases. T_g is associated with the flexibility of polymer chain segments.[43] This phenomenon may be attributed to the interaction between the components of the composite film, whereby CCNF facilitates the movement of the PVA chains.

As illustrated in the second heating run (Figure 6c), PVA underwent recrystallization on cooling. The crystallinity of the composite films was determined from the heat of fusion, as presented in Table 3. The crystallinity of the composite films exhibited an increase with the addition of CCNF. The observed increase in crystallinity of the composite films may be attributed to the nucleation effect of CCNF.[29]

3.7. Thermal Stability of Composite Films. Degradation of the composite films was divided into three stages (Table 4).

Table 3. Glass Transition Temperature (T_g), Melting Temperature (T_m), and Crystallinity (X_c) of PVA and CCNF/PVA Composite Films

samples	T_g (°C)	T_m (°C)	X_c (%)
PVA	70.22	177.96	14.99
2% CCNF/PVA	70.4	178.55	16.78
4% CCNF/PVA	69.85	177.25	14.91
8% CCNF/PVA	66.86	183.59	21.88
12% CCNF/PVA	66.45	185.35	24.01

The first stage from 28.14 to 138 °C was ascribed to the loss of adsorbed water (Figure 6d,e). The second stage from 138 to 361 °C was mainly caused by the decomposition of CCNFs and PVA side chains.[46,47] The third stage from 361 to 453 °C was mainly related to the degradation of the primary chain of PVA.[46,47] The addition of CCNFs did not appreciably alter the observed weight-loss behavior, implying that the CCNFs had no effect on the thermal stability of the PVA-based films. Overall, these films possess excellent thermal stability, making them suitable for packaging applications.

3.8. Mechanical Properties and Performance of Composite Films. Figure 6f shows the stress−strain curves of the composite films with different CCNF contents. The inclusion of CCNFs leads to notable increases of both the tensile strength and elongation at break of the films compared with those of the undoped PVA film. With the increase of CCNF content, the elongation at break of the composite films first increased and then decreased, reaching a maximum value of 612% when the CCNF content was 8%. The tensile strength increased from 36 MPa for pure PVA to 41.3 MPa for the composite films with 4 and 12% CCNFs.

The incorporation of CCNFs and their optimal distribution within the PVA film matrix resulted in the formation of hydrogen bonds between the CCNFs and PVA. Consequently, the mechanical properties of the films generally gradually

https://doi.org/10.1021/acsomega.4c05759
ACS Omega 2024, 9, 38205−38216

Table 4. Onset Temperature and Degradation Temperature (T_{max}) of PVA and CCNF/PVA Composite Films

	first process	second process		third process	
samples	T_{max} (°C)	onset temperature (°C)	T_{max} (°C)	onset temperature (°C)	T_{max} (°C)
PVA	104.28	140.79	314.62	368.38	384.72
2% CCNF/PVA	107.60	136.61	309.78	361.89	379.28
4% CCNF/PVA	118.77	138.18	313.94	360.51	383.79
8% CCNF/PVA	111.72	138.22	313.03	357.06	384.21
12% CCNF/PVA	108.02	135.74	310.24	352.72	382.03

improved with increasing CCNF content. However, the elongation at break decreased by 42% when the CCNF content of the composite film was 12%. This decrease was attributed to the high CCNF content, causing a concomitant decrease in dispersion and increase in aggregation. When this film was stretched in a region with aggregated CCNFs, localized stress concentration occurred, thus making it more susceptible to tensile damage.[27] The CCNF/PVA composite films show enhanced tensile strength and Young's modulus, along with greater stiffness and higher load-carrying ability, than those of an undoped PVA film. These results suggest that CCNFs prepared by the developed peroxyformic acid method are a promising reinforcing material for enhancing the mechanical strength of PVA-based films.[46]

4. CONCLUSIONS

In this study, CCNFs were prepared by a mild green preparation method involving delignification with peroxyformic acid, followed by alkali treatment and high-power ultrasonication. Characterization results showed that most of the lignin and hemicellulose of CF were effectively separated, amorphous regions were effectively hydrolyzed, and the prepared CCNFs had high crystallinity and high aspect ratio and were thermally stable up to around 300 °C. CCNF-reinforced PVA composite films showed improved mechanical performance compared with that of undoped PVA films without strongly affecting the surface morphology, transmittance, or thermal stability. This study demonstrates that CF has the potential as a source of NC for producing biodegradable composites with high tensile strength. These composites could be effective, environmentally friendly, and sustainable alternatives to synthetic composites and could have potential applications in packaging technology.

AUTHOR INFORMATION

Corresponding Authors

Gaofeng Pan − *Mudanjiang Hengfeng Paper Co., Ltd, Mudanjiang 157000, China*; Email: hengfengpaper6971@163.com

Shouxin Liu − *Engineering Research Center of Advanced Wooden Materials of the Ministry of Education, Northeast Forestry University, Harbin 150040, China*; orcid.org/0000-0002-0491-8885; Email: liushouxin@126.com

Wei Li − *Key Laboratory of Bio-Based Material Science and Technology of Ministry of Education, Northeast Forestry University, Harbin 150040, China*; orcid.org/0000-0002-3008-9865; Email: liwei19820927@126.com

Authors

Weishan Hou − *Key Laboratory of Bio-Based Material Science and Technology of Ministry of Education, Northeast Forestry University, Harbin 150040, China*

Rui Teng − *Key Laboratory of Bio-Based Material Science and Technology of Ministry of Education, Northeast Forestry University, Harbin 150040, China*; orcid.org/0009-0005-0614-0252

Aojia Zhang − *Key Laboratory of Bio-Based Material Science and Technology of Ministry of Education, Northeast Forestry University, Harbin 150040, China*

Bang An − *Key Laboratory of Bio-Based Material Science and Technology of Ministry of Education, Northeast Forestry University, Harbin 150040, China*

Mingcong Xu − *Key Laboratory of Bio-Based Material Science and Technology of Ministry of Education, Northeast Forestry University, Harbin 150040, China*

Chunhui Ma − *Key Laboratory of Bio-Based Material Science and Technology of Ministry of Education, Northeast Forestry University, Harbin 150040, China*; orcid.org/0000-0001-9590-3891

Complete contact information is available at: https://pubs.acs.org/10.1021/acsomega.4c05759

Author Contributions

W.H.: Data processing, investigation, and writing—original draft. R.T.: Test and data processing, writing—review and editing. A.Z.: Validation, supervision, funding acquisition. B.A.: Supervision, writing—review and editing, funding acquisition. M.X.: Supervision, writing—review and editing. C.M.: Supervision, writing—review and editing. G.P.: Supervision, writing—review and editing. S.L.: Supervision, writing—review and editing. W.L.: Methodology, validation, writing—review and editing.

Notes

The authors declare no competing financial interest.

ACKNOWLEDGMENTS

This work was financially supported by the National Natural Science Foundation of China (32071719) and the Fundamental Research Funds for the Central Universities (2572023CT06). The text was provided with language support by Edanz Institution (liwenbianji.cn).

REFERENCES

(1) Asasutjarit, C.; Charoenvai, S.; Hirunlabh, J.; Khedari, J. Materials and Mechanical Properties of Pretreated Coir-Based Green Composites. *Composites, Part B* **2009**, *40* (7), 633−637.

(2) Ru, S.; Zhao, C.; Yang, S. Multi-Objective Optimization and Analysis of Mechanical Properties of Coir Fiber from Coconut Forest Waste. *Forests* **2022**, *13* (12), 2033.

(3) Ferreira, P. F. O.; Pereira, A. L. S.; Rosa, M. F.; de Santiago-Aguiar, R. S. Lignin-Rich Cellulose Nanocrystals from Coir Fiber Treated with Ionic Liquids: Preparation and Evaluation as Pickering Emulsifier. *Ind. Crops Prod.* **2022**, *186*, No. 115119.

(4) Malladi, R.; Nagalakshmaiah, M.; Robert, M.; Elkoun, S. Importance of Agricultural and Industrial Waste in the Field of

Nanocellulose and Recent Industrial Developments of Wood Based Nanocellulose: A Review. *ACS Sustainable Chem. Eng.* **2018**, *6*, 2807−2828, DOI: 10.1021/acssuschemeng.7b03437.
(5) Ru, S.; Yang, R.; Yang, S.; Zhao, C. Effects of Physical and Mechanical Properties of Coir Fiber and Reinforced Epoxy Composites Treated with Acetic Anhydride and Alkali. *J. Nat. Fibers* **2023**, *20* (2), No. 2285819.
(6) Park, N.-M.; Choi, S.; Oh, J. E.; Hwang, D. Y. Facile Extraction of Cellulose Nanocrystals. *Carbohydr. Polym.* **2019**, *223*, No. 115114.
(7) Mohd Amin, K. N.; Annamalai, P. K.; Morrow, I. C.; Martin, D. Production of Cellulose Nanocrystals via a Scalable Mechanical Method. *RSC Adv.* **2015**, *5* (70), 57133−57140.
(8) Li, W.; Zhao, X.; Huang, Z.; Liu, S. Nanocellulose Fibrils Isolated from BHKP Using Ultrasonication and Their Reinforcing Properties in Transparent Poly (Vinyl Alcohol) Films. *J. Polym. Res.* **2013**, *20* (8), 210.
(9) Pavalaydon, K.; Ramasawmy, H.; Surroop, D. Comparative Evaluation of Cellulose Nanocrystals from Bagasse and Coir Agro-Wastes for Reinforcing PVA-Based Composites. *Environ., Dev. Sustain.* **2022**, *24* (8), 9963−9984.
(10) Chen, X.; Deng, X.; Shen, W.; Jiang, L. Controlled Enzymolysis Preparation of Nanocrystalline Cellulose from Pretreated Cotton Fibers. *BioResources* **2012**, *7* (3), 4237−4248.
(11) Wu, J.; Du, X.; Yin, Z.; Xu, S.; Xu, S.; Zhang, Y. Preparation and Characterization of Cellulose Nanofibrils from Coconut Coir Fibers and Their Reinforcements in Biodegradable Composite Films. *Carbohydr. Polym.* **2019**, *211*, 49−56.
(12) Yang, X.; Abe, K.; Yano, H.; Wang, L. Multifunctional Cellulosic Materials Prepared by a Reactive DES Based Zero-Waste System. *Nano Lett.* **2022**, *22* (15), 6128−6134.
(13) Shamsuri, A. A.; Md Jamil, S. N. A.; Abdan, K. Nanocellulose Extraction Using Ionic Liquids: Syntheses, Processes, and Properties. *Front. Mater.* **2022**, *9*, No. 919918.
(14) Leow, Y.; Boo, Y. J.; Lin, M.; Tan, Y. C.; Goh, R. Z. R.; Zhu, Q.; Loh, X. J.; Xue, K.; Kai, D. Coconut Husk-Derived Nanocellulose as Reinforcing Additives in Thermal-Responsive Hydrogels. *Carbohydr. Polym.* **2024**, *323*, No. 121453.
(15) Nascimento, D. M. D.; Almeida, J. S.; Vale, M. D. S.; Leitão, R. C.; Muniz, C. R.; Figueirêdo, M. C. B. D.; Morais, J. P. S.; Rosa, M. D. F. A Comprehensive Approach for Obtaining Cellulose Nanocrystal from Coconut Fiber. Part I: Proposition of Technological Pathways. *Ind. Crops Prod.* **2016**, *93*, 66−75.
(16) Mehanny, S.; Abu-El Magd, E. E.; Ibrahim, M.; Farag, M.; Gil-San-Millan, R.; Navarro, J.; El Habbak, A. E. H.; El-Kashif, E. Extraction and Characterization of Nanocellulose from Three Types of Palm Residues. *J. Mater. Res. Technol.* **2021**, *10*, 526−537.
(17) Thomas, B.; Raj, M. C.; B, A. K.; H, R. M.; Joy, J.; Moores, A.; Drisko, G. L.; Sanchez, C. Nanocellulose, a Versatile Green Platform: From Biosources to Materials and Their Applications. *Chem. Rev.* **2018**, *118* (24), 11575−11625.
(18) Wang, S.; Zou, Q.; Zhang, L.; Zheng, W.; Huang, X.; Zhang, J. A New Nanocellulose Prepared from Waste Coconut Shell Fibers Based on a Novel Ultrasonic—Active Agent Combination Method: Preparation Principle and Performances in Cement Matrix. *Ind. Crops Prod.* **2023**, *197*, No. 116607.
(19) Perez, D. D. S.; Terrones, M. G. H.; Grelier, S.; Nourmamode, A.; Castellan, A.; Ruggiero, R.; Machado, A. E. H. Peroxyformic Acid Pulping of Eucalyptus Grandis Wood Chips and Sugar Cane Bagasse in One Stage and Characterization of the Isolated Lignins. *J. Wood Chem. Technol.* **1998**, *18* (3), 333−365.
(20) Li, Z.; Chen, C.; Xie, H.; Yao, Y.; Zhang, X.; Brozena, A.; Li, J.; Ding, Y.; Zhao, X.; Hong, M.; Qiao, H.; Smith, L. M.; Pan, X.; Briber, R.; Shi, S. Q.; Hu, L. Sustainable High-Strength Macrofibres Extracted from Natural Bamboo. *Nat. Sustain.* **2022**, *5* (3), 235−244.
(21) do Nascimento, D. M.; Nunes, Y. L.; de Almeida, J. S.; Leitão, R. C.; Feitosa, J. P. A.; Dufresne, A.; Rosa, M. de F. Development of an Integrated Process to Produce CNFs and Lignin and Its Potential Applications for Agrochemical Delivery. *Cellulose* **2021**, *28* (17), 10891−10904.
(22) Tian, H.; Yan, J.; Rajulu, A. V.; Xiang, A.; Luo, X. Fabrication and Properties of Polyvinyl Alcohol/Starch Blend Films: Effect of Composition and Humidity. *Int. J. Biol. Macromol.* **2017**, *96*, 518−523.
(23) Thayumanavan, N.; Tambe, P.; Joshi, G.; Shukla, M. Effect of Sodium Alginate Modification of Graphene (by 'Anion- π' Type of Interaction) on the Mechanical and Thermal Properties of Polyvinyl Alcohol (PVA) Nanocomposites. *Compos. Interfaces* **2014**, *21* (6), 487−506.
(24) Usman, A.; Hussain, Z.; Riaz, A.; Khan, A. N. Enhanced Mechanical, Thermal and Antimicrobial Properties of Poly (Vinyl Alcohol)/Graphene Oxide/Starch/Silver Nanocomposites Films. *Carbohydr. Polym.* **2016**, *153*, 592−599.
(25) Wong, K. K. H.; Zinke-Allmang, M.; Hutter, J. L.; Hrapovic, S.; Luong, J. H. T.; Wan, W. The Effect of Carbon Nanotube Aspect Ratio and Loading on the Elastic Modulus of Electrospun Poly (Vinyl Alcohol)-Carbon Nanotube Hybrid Fibers. *Carbon* **2009**, *47* (11), 2571−2578.
(26) Deepa, B.; Abraham, E.; Cordeiro, N.; Mozetic, M.; Mathew, A. P.; Oksman, K.; Faria, M.; Thomas, S.; Pothan, L. A. Utilization of Various Lignocellulosic Biomass for the Production of Nanocellulose: A Comparative Study. *Cellulose* **2015**, *22* (2), 1075−1090.
(27) Li, W.; Wu, Q.; Zhao, X.; Huang, Z.; Cao, J.; Li, J.; Liu, S. Enhanced Thermal and Mechanical Properties of PVA Composites Formed with Filamentous Nanocellulose Fibrils. *Carbohydr. Polym.* **2014**, *113*, 403−410.
(28) Segal, L.; Creely, J. J.; Martin, A. E.; Conrad, C. M. An Empirical Method for Estimating the Degree of Crystallinity of Native Cellulose Using the X-Ray Diffractometer. *Text. Res. J.* **1959**, *29* (10), 786−794.
(29) Lu, J.; Wang, T.; Drzal, L. T. Preparation and Properties of Microfibrillated Cellulose Polyvinyl Alcohol Composite Materials. *Composites, Part A* **2008**, *39* (5), 738−746.
(30) Okita, Y.; Saito, T.; Isogai, A. Entire Surface Oxidation of Various Cellulose Microfibrils by TEMPO-Mediated Oxidation. *Biomacromolecules* **2010**, *11* (6), 1696−1700.
(31) Nascimento, D. M.; Almeida, J. S.; Dias, A. F.; Figueirêdo, M. C. B.; Morais, J. P. S.; Feitosa, J. P. A.; Rosa, M. de F. A Novel Green Approach for the Preparation of Cellulose Nanowhiskers from White Coir. *Carbohydr. Polym.* **2014**, *110*, 456−463.
(32) Arun, R.; Shruthy, R.; Preetha, R.; Sreejit, V. Biodegradable Nano Composite Reinforced with Cellulose Nano Fiber from Coconut Industry Waste for Replacing Synthetic Plastic Food Packaging. *Chemosphere* **2022**, *291*, No. 132786.
(33) Zhao, Y.; Xu, C.; Xing, C.; Shi, X.; Matuana, L. M.; Zhou, H.; Ma, X. Fabrication and Characteristics of Cellulose Nanofibril Films from Coconut Palm Petiole Prepared by Different Mechanical Processing. *Ind. Crops Prod.* **2015**, *65*, 96−101.
(34) Teng, R.; Sun, J.; Nie, Y.; Li, A.; Liu, X.; Sun, W.; An, B.; Ma, C.; Liu, S.; Li, W. An Ultra-Thin and Highly Efficient Electromagnetic Interference Shielding Composite Paper with Hydrophobic and Antibacterial Properties. *Int. J. Biol. Macromol.* **2023**, *253*, No. 127510.
(35) Himmelsbach, D. S.; Khalili, S.; Akin, D. E. The Use of FT-IR Microspectroscopic Mapping to Study the Effects of Enzymatic Retting of Flax (Linum Usitatissimum L) Stems. *J. Sci. Food Agric.* **2002**, *82* (7), 685−696.
(36) Jiang, F.; Hsieh, Y.-L. Chemically and Mechanically Isolated Nanocellulose and Their Self-Assembled Structures. *Carbohydr. Polym.* **2013**, *95* (1), 32−40.
(37) Xiao, B.; Sun, X. F.; Sun, R. Chemical, Structural, and Thermal Characterizations of Alkali-Soluble Lignins and Hemicelluloses, and Cellulose from Maize Stems, Rye Straw, and Rice Straw. *Polym. Degrad. Stab.* **2001**, *74* (2), 307−319.
(38) Li, W.; Yue, J.; Liu, S. Preparation of Nanocrystalline Cellulose via Ultrasound and Its Reinforcement Capability for Poly (Vinyl Alcohol) Composites. *Ultrason. Sonochem.* **2012**, *19* (3), 479−485.
(39) Gröndahl, M.; Teleman, A.; Gatenholm, P. Effect of Acetylation on the Material Properties of Glucuronoxylan from Aspen Wood. *Carbohydr. Polym.* **2003**, *52* (4), 359−366.

(40) Zhao, H.-P.; Feng, X.-Q.; Gao, H. Ultrasonic Technique for Extracting Nanofibers from Nature Materials. *Appl. Phys. Lett.* **2007**, *90* (7), No. 073112.
(41) d'Almeida, A. L. F. S.; Barreto, D. W.; Calado, V.; d'Almeida, J. R. M. Thermal Analysis of Less Common Lignocellulose Fibers. *J. Therm. Anal. Calorim.* **2008**, *91* (2), 405−408.
(42) Chen, W.; Yu, H.; Liu, Y.; Chen, P.; Zhang, M.; Hai, Y. Individualization of Cellulose Nanofibers from Wood Using High-Intensity Ultrasonication Combined with Chemical Pretreatments. *Carbohydr. Polym.* **2011**, *83* (4), 1804−1811.
(43) Osolnik, U.; Vek, V.; Korošec, R. C.; Oven, P.; Poljanšek, I. Integration of Wood-Based Components—Cellulose Nanofibrils and Tannic Acid into a Poly (Vinyl Alcohol) Matrix to Improve Functional Properties. *Int. J. Biol. Macromol.* **2024**, *256*, No. 128495.
(44) Lee, H.; You, J.; Jin, H.-J.; Kwak, H. W. Chemical and Physical Reinforcement Behavior of Dialdehyde Nanocellulose in PVA Composite Film: A Comparison of Nanofiber and Nanocrystal. *Carbohydr. Polym.* **2020**, *232*, No. 115771.
(45) Choo, K.; Ching, Y. C.; Chuah, C. H.; Julai, S.; Liou, N.-S. Preparation and Characterization of Polyvinyl Alcohol-Chitosan Composite Films Reinforced with Cellulose Nanofiber. *Materials* **2016**, *9* (8), 644.
(46) Liu, D.; Sun, X.; Tian, H.; Maiti, S.; Ma, Z. Effects of Cellulose Nanofibrils on the Structure and Properties on PVA Nanocomposites. *Cellulose* **2013**, *20* (6), 2981−2989.
(47) Yang, M.; Zhang, X.; Guan, S.; Dou, Y.; Gao, X. Preparation of Lignin Containing Cellulose Nanofibers and Its Application in PVA Nanocomposite Films. *Int. J. Biol. Macromol.* **2020**, *158*, 1259−1267.

https://doi.org/10.1021/acsomega.4c05759
ACS Omega 2024, 9, 38205−38216